Ice water content of Arctic, midlatitude, and tropical cirrus

C. Schiller,[1] M. Krämer,[1] A. Afchine,[1] N. Spelten,[1] and N. Sitnikov[2]

Received 30 April 2008; revised 7 July 2008; accepted 27 August 2008; published 24 December 2008.

[1] In situ measurements of total water have been obtained during several airborne field experiments in the Arctic (POLSTAR 1997 and 1998; EUPLEX/ENVISAT 2003), at midlatitudes (ENVISAT 2002, Cirrus 2003 and 2004, TROCCINOX 2005), and in the tropics (APE-THESEO 1999, TROCCINOX/ENVISAT 2005, SCOUT-O3 2005) in 52 flights in cirrus using the Jülich Lyman-α fluorescence hygrometer FISH. For a subset of 28 flights, the measurements are complemented by gas phase measurements of H_2O. From the data set obtained in these experiments, the ice water content (IWC) in cirrus clouds is derived using two different approaches and functions of the minimum, mean, median, and maximum IWC are provided. The data are analyzed as a function of temperature in the range 183–250 K for Arctic, midlatitudinal, and tropical regions thus extending previous climatologies to much lower temperatures and lower detectable IWC. For each temperature, IWC covers a broad band, decreasing with temperature over the whole temperature range. In the tropics, several events of enhanced ice water content are observed which are related to recent impact of convection.

Citation: Schiller, C., M. Krämer, A. Afchine, N. Spelten, and N. Sitnikov (2008), Ice water content of Arctic, midlatitude, and tropical cirrus, *J. Geophys. Res.*, *113*, D24208, doi:10.1029/2008JD010342.

1. Introduction

[2] Cirrus clouds are an important factor in the Earth's climate system, though their microphysical and radiative properties are still not well characterized [*Forster et al.*, 2007]. They play an important role in the water budget of the upper troposphere and are thus regulating the humidity of air entering the stratosphere. Cirrus clouds further impact the chemical composition of the tropopause region by heterogeneous reaction of nitrogen and halogen species on their surfaces resulting in a destruction of ozone [*Borrmann et al.*, 1996]. In this context, the uptake of HNO_3 in cirrus ice clouds has been subject of several studies [e.g., *Krämer et al.*, 2008a, and references therein].

[3] The ice water content (IWC) of cirrus clouds strongly impacts their radiative properties [e.g., *Fu*, 1996] as well as the upper tropospheric water budget [e.g., *Fueglistaler and Baker*, 2006] and chemistry. The IWC may vary over several orders of magnitude for different cirrus clouds, depending on available water, temperature, cooling rate, and likely also on the number and composition of available ice nuclei.

[4] Cirrus clouds are observed at all latitudes in the cold upper troposphere and close to the tropopause. The temperatures in this altitude region is, however, highly variable: At midlatitudes, they typically do not fall much below 210 K, while at polar latitudes, tropopause temperatures around 200 K and below can occur. The coldest temperatures, down to 185 K, are observed at the tropical tropopause, resulting in a very efficient freeze-drying of air passing these regions.

[5] Here, we determine IWC of cirrus clouds from airborne observations of total water and gas phase water at Arctic, midlatitude, and tropical regions. We derive a climatology of the IWC for the different latitudes and discuss their temperature dependence over a wide range of temperatures down to 185 K, thus extending previous climatologies of IWC for midlatitudes [*Heymsfield and Platt*, 1984; *Wang and Sassen*, 2002; *Gayet et al.*, 2006] for tropical and polar conditions and lower IWC. We discuss the impact of specific events such as convection on the IWC. In two upcoming papers, this climatology will be used to derive further climatologies, first of HNO_3 uptake in cirrus clouds [*Krämer et al.*, 2008a] and, second, of water vapor supersaturations inside cirrus [*Krämer et al.*, 2008b]. A third paper introduces IWC climatologies in a radiative transfer code to reinvestigate contrail radiative forcing (Rodriguez et al., manuscript in preparation, 2008).

2. Experiment

[6] The total water measurements used in this study have been performed by means of the Fast In Situ Stratospheric Hygrometer (FISH), which is based on the Lyman-α photofragment fluorescence technique. A detailed description of this instrument and its characteristics is given by *Zöger et al.* [1999]. We use two distinct FISH instruments differing only in the mechanical set up adapted to the aircraft types on which they are operated. FISH is sensitive for H_2O mixing ratios from approximately 0.5 to 1000 ppmv and thus well suited for investigations in the UTLS over a large dynamical range. The time resolution is 1 s, determined by the exchange time of air through the measurement cell. With

[1] Institut für Chemie und Dynamik der Geosphäre 1, Forschungszentrum Jülich, Stratosphäre, Germany.
[2] Central Aerological Observatory, Dolgoprudny, Russia.

0148-0227/08/2008JD010342

Table 1. Listing of Arctic, Midlatitude, and Tropical Field Campaigns[a]

Campaign	Base	Time	Aircraft	Flight Dates[b]
POLSTAR I	Kiruna, 68°N	Jan 1997	Falcon	0124
POLSTAR II	Kiruna, 68°N	Jan 1998	Falcon	0126
			Lear Jet	0126
EUPLEX	Kiruna, 68°N	Jan–Feb 2003	Geophysica	0115[c] 0126 0208[c] 0209 0211
ENVISAT II	Kiruna, 68°N	Mar 2003	Geophysica	0302[c] 0316[c]
ENVISAT I	Forli', 44°N	Oct 2002	Geophysica	1008[c] 1011 1014 1017[c] 1022
Cirrus I	Hohn, 54°N	Dec 2003	Lear Jet	1212[d] 1213[d]
Cirrus II	Hohn, 54°N	Nov 2004	Lear Jet	1124[d] 1127[d]
Cirrus III	Hohn, 54°N	Nov 2006	Lear Jet	1123 1124[d] 1128[d] 1128[d] 1129[d]
TROCCINOX-M	Oberpfaffenhofen, 48°N	Jan/Mar 2005	Geophysica	0118 0307
APE-THESEO	Seychelles, 5°S	Feb–Mar 1999	Geophysica	0219[c] 0224 0227 0304 0309[c] 0311
TROCCINOX	Araçatuba, 21°S	Jan–Feb 2005	Geophysica	0123 0127[c] 0201[c] 0204 0205 0208 0217 0218[c] 0224[c]
SCOUT-O3	Darwin, 12°S	Nov–Dec 2005	Geophysica	1107[c] 1109[c] 1111[c] 1112[c] 1119[c] 1123[c] 1125 1129 1130[c] 1130[c]
			Falcon	1128 1129 1130

[a]Arctic: POLSTAR I and II, EUPLEX, ENVISAT II; midlatitude: ENVISAT I, Cirrus I and II; tropical: APE-THESEO, TROCCINOX, SCOUT-O3. The TROCCINOX and SCOUT-O3 data are obtained during flights from the listed base as well as during the tropical part of the transfer route to or from Europe.
[b]Flights in cirrus clouds, format MMDD.
[c]Gas phase measurements from FLASH available.

this integration time, the detection system can resolve changes of H_2O on the order of 0.1 ppmv or 3%.

[7] Calibration of the hygrometers is made using a calibration bench, consisting of a system to generate air of different humidity and pressure [*Zöger et al.*, 1999]. The reference for this calibration is a frost point hygrometer (MBW DP30) whose calibration is regularly checked with that of reference instruments. Calibration of FISH during campaign deployment is usually repeated after each flight with this calibration bench. The overall accuracy of water vapor measurements with FISH is 6% or at least 0.3 ppmv. FISH has also been compared to other in situ hygrometers and remote sensing instruments in atmospheric measurements [e.g., *Kley et al.*, 2000, and references therein].

[8] Since FISH is a closed-cell instrument, the air is probed by a forward facing inlet tube mounted outside of the research aircraft. The inlet thus samples total water, i.e., the sum of both gas-phase molecules and ice particles. The large ice particles are sampled with enhanced efficiency compared to the gas molecules [*Schiller et al.*, 1999]. The sampling characteristics for the inlets of the different research aircraft have been determined by computational fluid dynamics modeling [*Krämer and Afchine*, 2004]. As shown in these publications, the aspiration coefficient (or enhancement factor) of our aircraft inlets increases from its minimum value (i.e., 1–2) for particles with radii smaller than 0.3 μm to its maximum value E_{max} which is typically achieved for particle radii larger than 3–4 μm. E_{max} is the ratio of the flow velocity inside the inlet U_{inlet} and the free flow U_0. The calculation of the aspiration factor has been made for typical flow velocities U_{inlet} and U_0 as they occur during the airborne measurements. For ice crystals, the maximum aspiration factor for large particle radii E_{max} can be used in first approximation since most water is condensed in these larger particles [*Schiller et al.*, 1999], and the contribution of water from smaller particles sampled with the enhancement 1–2 can be neglected. In the data evaluation today, we apply enhancement factors from the actual flow velocities along the flight track, where $U_{inlet} = q/A$ is determined from the flow q measured in the instrument and the inlet cross-section area A. For our inlets, E_{max} ranges from approximately 3 (Lear Jet) to 8–10 (Geophysica aircraft). The precision for the determination of the enhancement factor is estimated to 0.1, based on sensitivity studies of the fluid dynamics calculations.

[9] During part of the flights, also gas phase measurements of H_2O using the Lyman-α Stratospheric Hygrometer FLASH of the Central Aerological Observatory [*Sitnikov et al.*, 2007] and the open-path tunable diode laser spectrometer OJSTER of Forschungszentrum Jülich [*Schlicht*, 2006] are available (see Table 1). For this subset of 28 flights, we derive IWC as the difference between the total water measurement and the gas phase measurement, divided by the enhancement factor E_{max}: $IWC = (H_2O_{tot} - H_2O_{gas})/E_{max}$. The gas phase measurements will also be used in a study on supersaturations [*Krämer et al.*, 2008b]. FLASH uses an inlet with a kinetic separation for particles and thus allows for a gas phase measurement as calculated by fluid dynamic simulations and demonstrated during selected flights [*Sitnikov et al.*, 2007]. It is calibrated with a similar device as FISH, the accuracy is 8%. For 1 s data, FLASH has lower signal-to-noise ratio compared to FISH. OJSTER is using the same technique and data analysis routines as the JPL spectrometer [*May*, 1998], its nominal accuracy for 1 s measurements is 5%.

[10] The error of IWC, which is calculated from the difference to the total water measurements of FISH and the gas phase measurement by FLASH or OJSTER, is minimized by adjustment of the FLASH and OJSTER data to those of FISH for observation periods outside clouds. Thus, systematic differences between the hygrometers are eliminated. Then, the uncertainty for the IWC is determined mainly by the accuracy of the FISH measurement and of the aspiration coefficient for the sampling efficiency of particles, plus the precision of the gas phase measurement whose impact on the IWC data set is discussed in section 3.

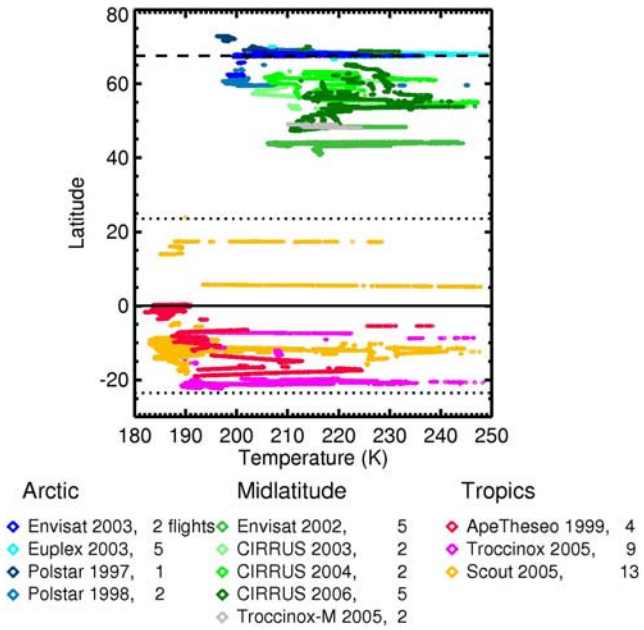

Figure 1. Data coverage of observed ice clouds as a function of latitude and temperature. Data points represent 27.0 flight hours inside cirrus clouds during 52 flights in the Arctic, at midlatitudes, and in the tropics.

The overall uncertainty of the IWC varies from 7% to 20%; the highest uncertainties above 10% are calculated for very low IWC observed below 190 K. For larger IWC ($>10^{-4}$ g/cm^3), the IWC derived from our H_2O measurements has been compared to that of particle probe data (combined FSSP and CIP) resulting in an agreement within the combined error bars of both methods [*de Reus et al.*, 2008].

[11] The ice water content can alternatively be determined as the difference between the FISH total water measurement and the water vapor saturation mixing ratio (see below), divided by the enhancement factor: IWC = (H_2O_{tot} − H_2O_{sat}(T))/E_{max}. Hereby, the saturation mixing ratio is determined from pressure and temperature measurement onboard the aircraft. The accuracy of these systems is specified by the operators of the Falcon and LearJet aircraft, DLR and enviscope, respectively, as 0.5 K for the temperature and 1 hPa for the pressure measurement. For the Geophysica, the same accuracy is achieved for the pressure data; for temperature, which is measured by the thermodynamic complex (TDC) since the EUPLEX project in 2003, also 0.5 K accuracy is specified by the operator of this sensor (G. Shur, Central Aerological Observatory, Moscow, personal communication, 2003). For earlier campaigns, the onboard navigational system has been available only with an accuracy for temperature measurement of 0.8 K, estimated from comparison with the TDC in the following campaigns.

[12] With these experimental uncertainties, we calculate the uncertainty of the saturation mixing ratio based on the equation by *Marti and Mauersberger* [1993]. This uncertainty is ranges from 5 to 10% over the temperature range of the data set in this study. This error increases the uncertainty in the determination of the IWC, to which also the error of the measurement of total water and that of the aspiration coefficient contributes (see above).

[13] For this study, FISH data obtained during 10 field experiments are used which are listed in Table 1: In the Arctic winter, measurements were made during the Polar Stratospheric Aerosol Experiment (POLSTAR) 1997 and 1998 and during the European Polar Stratospheric Cloud and Lee Wave Experiment (EUPLEX) combined with the ENVISAT validation experiment in 2003. All Arctic flights were made from Kiruna in Northern Sweden (68°). For the investigation of midlatitude cirrus, data of the ENVISAT validation experiment in Forli', Italy (44°N) in 2002, the Cirrus campaigns in 2003 and 2004 from Hohn, Germany (54°N), and one flight at the end of the Tropical Convection, Cirrus and Nitrogen Oxides Experiment (TROCCINOX) 2005 from Oberpfaffenhofen, Germany (48°N) are used. Tropical cirrus were observed during the Third European Stratospheric Experiment on Ozone (APE-THESEO) measurements in 1999 over the Indian Ocean (5°S), the TROCCINOX measurements from Araçatuba, Brazil (21°S) and the Stratospheric-Climate Links with Emphasis on the UTLS (SCOUT-O3) campaign in Darwin, Australia (12°S) in 2005.

[14] In these projects, three different research aircraft are used as listed in Table 1: The Russian high-altitude aircraft M55 Geophysica with a maximum ceiling of 20 km (∼50 hPa) and a typical cruising speed of 200 m/s, the DLR Falcon and the GFD Lear Jet, both operating typically at 9–13 km (∼200 hPa) and cruising speeds around 220 m/s. With these aircraft, altitudes up to the temperature minimum at the tropopause could be probed at high and mid latitudes as well as in the tropics, the latter with the Geophysica only.

[15] During these experiments, cirrus observations were made on 52 flights (Table 1) with a total measurement time in cirrus of 27.0 h. Gas phase measurements are available for 28 flights and 12.7 h, respectively. On the basis of an aircraft cruising speed of 200 m/s the measurement time transforms into a distance of 19,400 km (full data set) or 9100 km for the combined total/gas phase data set. Figure 1 provides the temperatures at which cirrus clouds have been observed as a function of latitude. The measurements cover latitudes from 78°N to 22°S and a temperature range from 185 K to 250 K. Cirrus clouds at lowest temperatures were observed in the tropics, in particular during the Seychelles and Darwin experiments. Over Brazil, still temperatures down to 190 K occurred in single cases, while in the Arctic and at mid latitudes, temperatures in air masses containing cirrus usually did not drop below 195 K and 203 K, respectively.

3. Results

3.1. Cloud Detection

[16] Ice clouds, even those with low IWC, can be detected very sensitively from the total water measurements of FISH because of the oversampling efficiency of the inlet. The most crucial example are the ultrathin tropical cirrus clouds (UTTC) detected over the Indian Ocean during APE-THESEO with an IWC of less than 0.1 ppmv (at an ambient H_2O mixing ratio of approximately 3 ppmv) which still results in a significant signal in FISH total water measurement [*Luo et al.*, 2003, Figure 1 therein]. UTTC

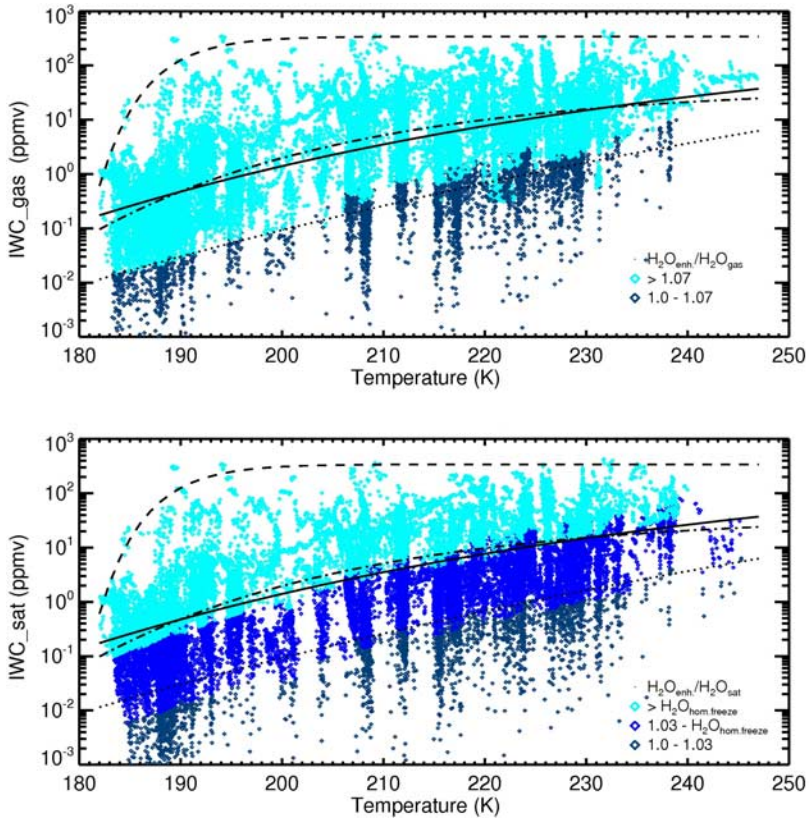

Figure 2. Ice water content during the 28 flights when both gas phase H_2O and total water measurements are available. (top) IWC determined as the difference of measured total and gas phase water (IWC_{gas}). Dark blue points represent data where the difference between both measurements is not significant to unambiguously identify a cloud. (bottom) IWC determined as the difference of measured total water and the saturation mixing ratio (RH_{ice} = 100%) from temperature and pressure measurement. The colors represent ranges of RH_{ice} of 100–103%, 103% to the homogeneous freezing threshold, and larger than this threshold, respectively. The black line is a fit of minimum IWC determined from 13 flights when gas phase measurements were available to allow for an unambiguous detection of clouds.

are the thinnest ice clouds so far observed in the lower and middle atmosphere.

[17] However, the detection of clouds and the determination of the IWC remain challenging. In this study, the ice water content is calculated in two ways, i.e., as the difference of the total hydrogen measurement and the gas phase measurement or, for the full data set, as the difference of the total hydrogen measurement and the saturation mixing ratio (100% RH_{ice}: relative humidity with respect to ice), divided by the enhancement factor (see section 2). We will discuss the differences of both approaches using the data set of 28 flights when also gas phase measurements are available: Figure 2 shows the IWC calculated from the difference of total water and gas phase measurement (IWC_{gas}, Figure 2, top) and calculated as the difference between total water measurement and the 100% saturation mixing ratio (IWC_{sat}, Figure 2, bottom) as a function of temperature.

[18] For the first approach, the criterion for the detection of clouds is the total water measurement exceeding that of the gas phase. In Figure 2 (top), we marked those data in dark colors for which the difference between both measurements is less than 7%. Owing to the combined precision of both measurements involved, those data cannot be unambiguously be discriminated and may either represent very thin clouds or an instrumental artifact. Figure 2 includes a dotted line representing the upper limit of these ambiguous data and will therefore be used as the minimum (detectable) IWC in the following. The fitted function and its coefficients are listed in Table 2 and provided as idl routines in the auxiliary material.[1] We recall that potential discrepancies between the instruments in terms of absolute calibration have been minimized by adjustment of the data in cloud-free conditions.

[19] For the second method, when using the saturation ratio (RHi = 100%) instead of gas phase measurements another uncertainty is inferred. Several recent laboratory, field and model studies imply that a substantial supersaturation can be maintained before a cloud forms or even in clouds [*Ovarlez et al.*, 2002; *Jensen et al.*, 2005; *MacKenzie et al.*, 2006]. However, the frequency of supersaturation decreases with the degree of supersaturation, and not all cirrus clouds exhibit supersaturation in the gas phase H_2O, as shown for our APE-THESEO data set [*MacKenzie et al.*, 2006, Figure 7]. For supersaturation conditions, the IWC derived by this method (IWC_{sat}) is overestimated. Con-

[1] Auxiliary materials are available in the HTML. doi:10.1029/2008JD010342.

Table 2. Fit Coefficients for Median, Mean, Maximum, and Minimum Approximations in Figures 3, 4, and 5[a]

Parameter	Temperature (K)	a	b	c
Minimum (28 flights)	183–250	−29.0184	0.992003	4.79070
Maximum (all flights)	183–250	−4.72212e+18	0.793983	2.53330
Median (28 flights, gas)	183–250	−2899.39	0.962236	1.60859
Median (28 flights, sat)	183–250	−2853.16	0.962268	1.59313
Median (all flights)	183–250	−68.4202	0.983917	2.81795
Mean (all flights)	183–250	−696056	0.932751	1.58834
Mean (without convection)	183–250	−1190.68	0.967686	2.15584
Median (Arctic)	197–250	−46885.7	0.952033	2.33488
Mean (Arctic)	197–250	−8025.809	0.960043	2.56690
Median (midlatitudes)	203–250	0.0231674		−4.22131
Mean (midlatitudes)	203–250	0.0166517		−2.48507
Median (tropics)	183–250	−23720.9	0.951279	1.52928
Mean (tropics)	183–250	−6.26765e08	0.899397	1.57802
Mean (tropics, without convection)	183–250	−21161.4	0.952294	1.82953
Core maximum (all flights)	183–250	−396248	0.937089	2.44491
Core minimum (all flights)	183–250	−54.3215	0.986506	2.57180

[a]The fitted functions of the IWC (in units ppmv) are $10^{(ab^{T}+c)}$, except for the midlatitude fits, when $10^{(aT+c)}$ has been used in analogy to previous climatologies. The functions, including their transformation to g/m^3 units, are provided as auxiliary material to this paper.

versely, for ice particles in subsaturated air, IWC will be underestimated with this approach. Observed frequency of RH_i distributions in cirrus [e.g., *Ovarlez et al.*, 2002] are peaking at RH_i = 100% with only a moderate asymmetry between higher and lower humidities, as also derived for our data set [*Krämer et al.*, 2008b]. Thus, both phenomena almost cancel each other in a climatological view of the data set.

[20] Nevertheless, an additional uncertainty might have to be added to that arising from instrumental uncertainties (including the determination of the saturation mixing ratio) discussed in section 2. The degree of the potential supersaturation varies with temperature, pressure, the water concentration, and other factors such as the number and size of ice crystals. Thus, the points of IWC in Figure 2 (bottom) may include data of supersaturated air masses without clouds. Vice versa ice particles in a subsaturated environment are missing when the total water signal does not exceed 100% RHi. For illustration, we color-coded the IWC data points in Figure 2 (bottom) for different ranges of RH_{ice}, i.e., 100–103%, 103% to the homogeneous freezing threshold, and higher than this threshold; hereby, RH_{ice} is calculated for each IWC data point from the raw, uncorrected total water signal. The IWC data in the lowest category (<103%) might be ambiguous also based on the instrumental accuracy. These lowest IWC data are very similar to those which have been discriminated in Figure 2 (top) when the difference of total water and gas phase measurement became too small to be detectable. Therefore, the detection limit derived above (dotted line) can be applied for the second approach as well. Part of the data up to the homogeneous freezing threshold (in Figure 2, bottom) can be overestimated as discussed. However, as both methods yield a very similar IWC distributions (no large discrepancies observable between Figure 2, top and bottom), only a smaller fraction of the data seems to be affected by supersaturation to a larger degree. Considering the oversampling of the total water measurement, the subtraction of a sometimes overestimated or underestimated baseline becomes significant only for very low IWC anyway. This can explain the somewhat higher frequency of the lowest IWC data in Figure 2 (bottom) compared to Figure 2 (top). This phenomenon therefore seems to overcompensate that of the potentially missing data of particles in subsaturated air.

[21] We note that particle observations to discriminate between in-cloud and cloud-free conditions are not available for all missions used in this study or might not be of sufficient sensitivity for the lowest IWC. Therefore, such measurements have not been considered in this climatological study.

3.2. IWC Climatologies

[22] For the forthcoming discussion in this paper, we derive mean and median values for each 2K-temperature bin. These values are then fitted using a function of the form $10^{(ab^{T}+c)}$ in order to match the steep decrease of IWC at low temperatures; coefficients for the different fit functions are listed in Table 2. A second-order polynomial function, as, e.g., used in the midlatitude climatology by *Wang and Sassen* [2002], or a linear exponential function $10^{(aT+c)}$ as fitted by *Kärcher and Voigt* [2006] to this particular data set, do not properly fit the strong temperature dependence over the extended temperature range of our study in many cases. However, when parameter b is close to 1, the function $10^{(ab^{T}+c)}$ is approximated by a linear exponential function of the form $10^{(aT+c)}$. For several fits below (see parameter b in Table 2), this approximation can still be used.

[23] The fits of the median are plotted in Figure 2 as dashed-dotted lines (solid lines denote the median for the full data set as a reference, see below). The median fits are very similar for both approaches; see also the coefficients in Table 2. Owing to the similarity of both approaches, it is worth to extend the study in the following to the full data set of 52 flights and to determine IWC from the difference between total water and the saturation mixing ratio (as gas phase measurements are not available for all flights). The maximum IWC are approximated by upper envelopes

(dashed lines in Figure 2), which are the same for both approaches as well as for the full data set.

[24] With the extended data set, statistics will be improved and thus allow to assess the climatological character of our data set. For comparison, Figure 2 also includes the median fit for the complete data set (solid line). It agrees well with the fitted curves of the reduced data set with 28 flights in terms of their absolute values but has a slightly reduced curvature (determined by coefficient b in Table 2). The similarity of the fits implies that they, despite the limited sampling volume, already include a representative selection of atmospheric conditions and cirrus cloud types, as adding or removal of individual flight or campaigns do not impact the median fit strongly. In particular, the similarity of both data sets also implies that no obvious bias from the flight pattern of the aircraft is noticeable, neither with a preference flying in subsaturated conditions (potentially shifting the statistics toward lower IWC) nor with a preference flying in supersaturated areas. We will however discuss examples below, how extreme cases as convection influence the IWC distribution, and also potential discrepancies to other climatologies based on different experimental approaches.

[25] The striking feature in Figure 2 is the strong temperature dependence of the ice water content with temperature. Despite a large variability of IWC over several magnitudes for a single temperature bin, the mean IWC decreases with decreasing temperatures. Figure 3 displays the IWC versus temperature, binned for the Arctic, midlatitude, and tropical campaigns. Again, we display the fitted mean as well as the median for each of the data sets in order to illustrate the general change in IWC with temperature. For a first discussion, all data are considered, and extreme values which are caused by specific situations such as convection (see section 4) are less weighted using the median.

[26] The midlatitude data in Figure 3 (middle) cover a temperature range of 203 to 250 K. They represent 16 flights with a total of 10.6 flight hours in cirrus clouds or corresponding to a flight route of 7600 km. In this data set, the dependence of the fitted mean IWC with temperature is quasi-linear in the exponent and decreasing with temperature. Such a linear dependence in the exponent, as also used in the work of *Kärcher and Voigt* [2006] derived from the data set of *Wang and Sassen* [2002], is the approximation of our fit function when the coefficient b becomes close to 1 (see Table 2).

[27] The median value of the IWC for the midlatitude data subset is 4–40 ppmv, that of the mean is 10–70 ppmv. The data are compared with other midlatitude climatologies of IWC: *Wang and Sassen* [2002] derived a climatology from a combined lidar-radar data set in the same temperature range, displayed by the hatched line in Figure 3. The mean IWC of Wang and Sassen show only a slightly stronger slope with temperature than ours and a remarkable good absolute agreement. This agreement is not necessarily expected as the applied remote techniques likely results in biases compared to our in situ data set, e.g., the low sensitivity of the radar to thin cirrus clouds or the occultation of a lidar beam by lower clouds masking overlaying (thin) cirrus. The suppression of low IWC might however be less important when comparing the mean which is provided in the Wang and Sassen publication. The similarity of the slopes gives further confidence, that our data with lower coverage compared to the 1000 h of measurement in the Wang and Sassen study is representative for larger parts of the atmosphere. A thousand hours of ground-based measurements translate in a linear distance on the order of 36,000 km (assuming a mean wind speed of 10 m/s for the upper troposphere at midlatitudes); thus our midlatitude data set with 7600 km flight route in clouds is lower but of the same order of magnitude. Our full data set with 20,000 km, however spread over a large latitude belt, has a very similar spatial extension as that of Wang and Sassen.

[28] *Gayet et al.* [2006] determine the temperature dependence of IWC using in situ particle measurements from aircraft at Southern Hemisphere midlatitudes. These data are integrated ice number densities from a set of three instruments from 3 μm to the millimeter diameter range. The authors also found a decrease of the IWC from 250 K to 213 K. They calculated median IWC data which are overlaid in Figure 3. However, these IWC are systematically higher than ours by a factor of 1.5 to 3. The major part of this discrepancy may be caused by methodological uncertainties on the order of a factor 2 when calculating IWC from size distribution measurements [e.g., *Heymsfield and McFarquhar*, 2002; *de Reus et al.*, 2008]. A comprehensive cirrus climatology from different field experiments using in situ size distribution measurements is compiled by *Heymsfield and McFarquhar* [2002] which *Gayet et al.* [2006] compare with their data. Though Heymsfield and McFarquhar consider only particles larger than 100 μm diameter in their analysis (which represent the major fraction of IWC under these conditions), a good agreement was found to the Gayet et al. data. In summary, our IWC data set at midlatitudes is broadly consistent with that of Wang and Sassen (for the mean) but systematically lower than that of Gayet et al. (for the median). The latter data set also considers thin clouds with low IWC which are suppressed in the climatologies of Wang and Sassen and Heymsfield and McFarquhar due to experimental reasons.

[29] The Arctic data (Figure 3, top) are taken from 10 flights with 3.5 flight hours in clouds (2550 km flight route). The Arctic data are the smallest subset of our data record, and in particular for the higher temperatures the data might be too sparse to make a climatological analysis. On the other hand, a considerable amount of data down to 197 K are obtained extending the range of our midlatitude climatology and that of *Wang and Sassen* [2002] and *Gayet et al.* [2006] to lower temperatures. Here, a stronger drop of the IWC is apparent for the mean and the median. It is worth to note that also the maximum values for temperatures below 215 K are already lower than those at midlatitudes. The median and mean IWC values at temperatures of 198–205 K are only 0.8–4 ppmv and 1.5–5 ppmv, respectively.

[30] Lowest temperatures down to approximately 185 K were measured during the tropical campaigns (Figure 3, bottom). Here, data from 26 flights and 12.9 h in clouds corresponding to 9300 km flight route are considered. When selecting flights without convective events (see below), the median and mean of IWC drop below 1 ppmv below 195 K and decrease further by about one order of magnitude toward the lowest temperatures. Below 200 K, IWC of several ppmv occur only in selected events which can be

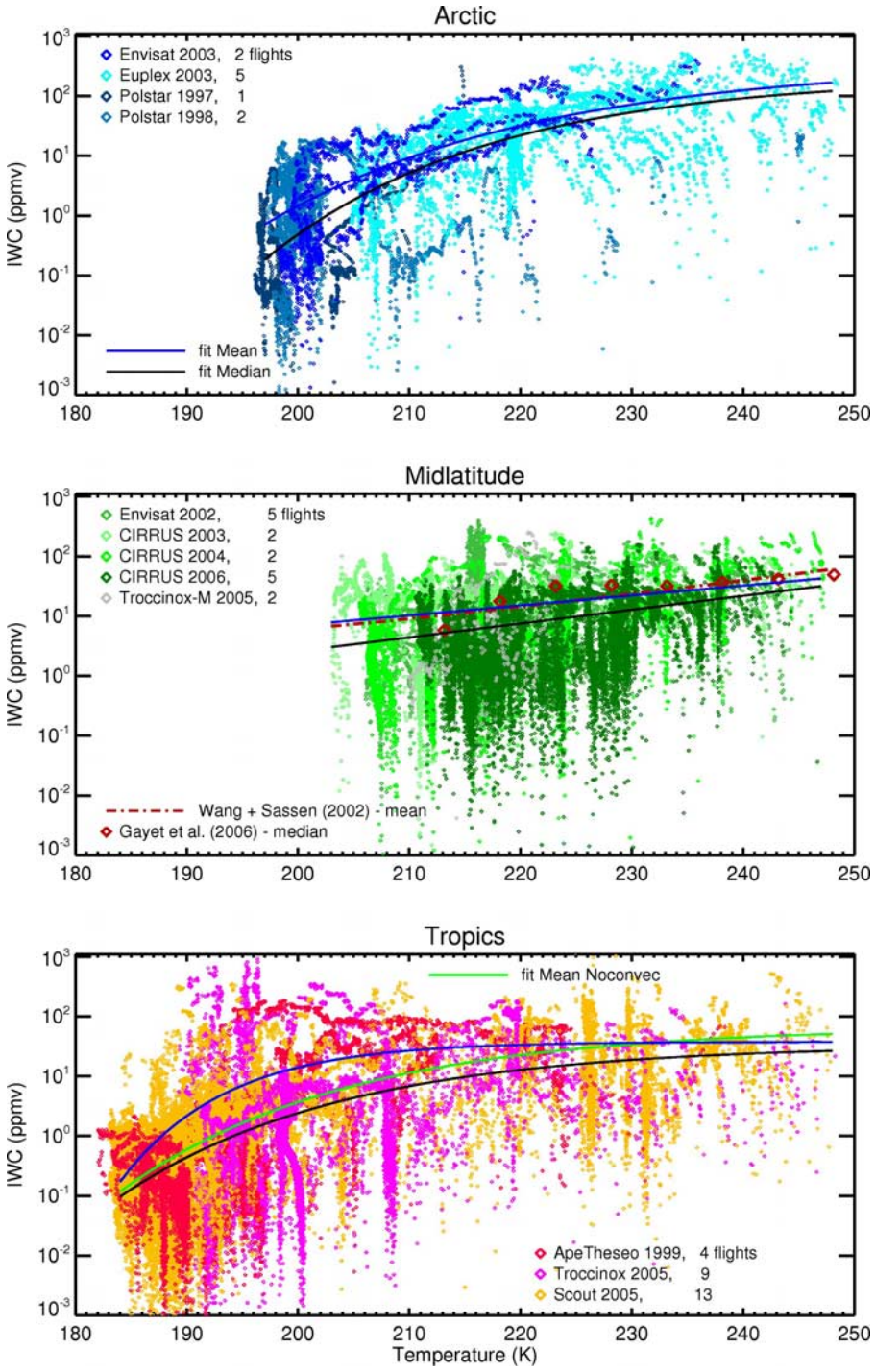

Figure 3. Ice water content (IWC) as a function of temperature, binned for (top) Arctic, (middle) midlatitude, and (bottom) tropical measurements. Black/blue/green lines are fits through the median/mean/mean (without convective events) values. In Figure 3 (middle), the hatched line denotes the mean of the IWC climatology at midlatitudes by *Wang and Sassen* [2002] and that of *Gayet et al.* [2006].

attributed to convective cirrus (see section 4). A climatological study for tropical cirrus by *McFarquhar and Heymsfield* [1997] is broadly consistent with the observed drop in average IWC to lower temperatures; however, this data set is restricted to temperatures down to 205 K only as the aircraft did not reach the cold point altitude. IWC values estimated for individual thin tropical tropopause clouds confirm the further drop with decreasing temperature [e.g., *Heymsfield*, 1986].

[31] To show the vertical distribution of cirrus clouds, Figure 4 displays the temperature versus geometrical altitude profiles in the observed cirrus clouds of our data set. The data reflect the known differences of the atmospheric structure in the three latitude regions, and they show that

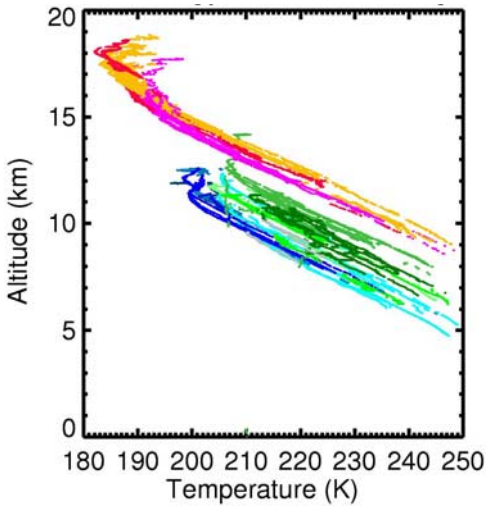

Figure 4. Vertical distribution of temperature in cirrus cloud observations. Color codes (as in Figures 3 and 5) denote the individual flights (red/orange denotes the tropics; green denotes midlatitudes, and blue denotes Arctic).

cirrus clouds are observed up to the cold point and in several cases even 1–1.5 km above. At all latitudes, lowest IWC are observed close to the local tropopause, i.e., at the cold point, which is around 10–13 km (330 K potential temperature) for middle and high latitudes and around 17 km (380 K potential temperature) for the tropics. IWC larger than 1 ppmv occur only up to the cold point, except for a few cases of deep convection penetrating the tropopause (see below), while in the lower stratosphere, the IWC of cirrus clouds are typically below 1 ppmv.

[32] Figure 5 summarizes the data of IWC from all campaigns, both for mass (Figure 5, top) and volume mixing ratios (Figure 5, bottom). The same color codes as in Figure 3, i.e., bluish colors for Arctic, greenish for midlatitude, and orange/reddish colors tropical data, are used for the individual campaigns. The fit of the mean and the median considering all data is very similar to that of the tropical data subset. The individually fitted mean and median for the Arctic and midlatitude data compare well with that of the complete set in the higher temperature range. As discussed in section 4, five tropical flights were made in the vicinity of deep convection and resulting in unusually high IWC. For the determination of the mean

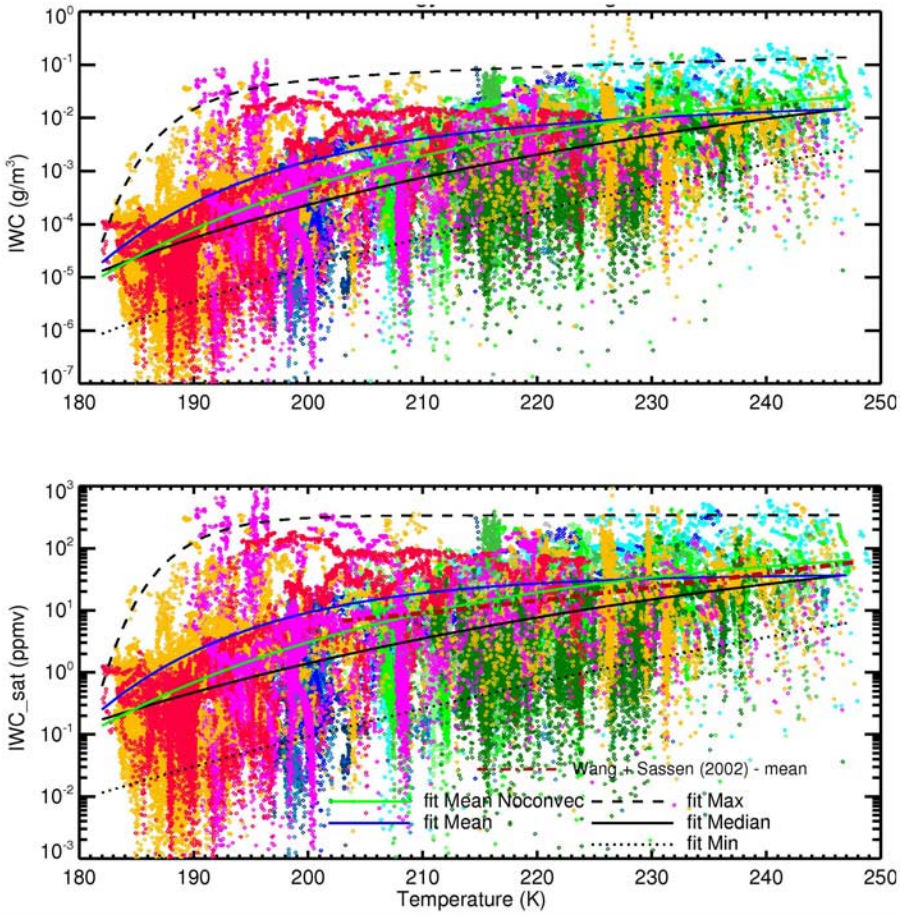

Figure 5. Ice water content (IWC) of cirrus clouds versus temperature from all Arctic, midlatitude, and tropical campaigns. Color codes denote the individual campaigns, chosen as in Figure 3. The solid black/blue/green lines are the fitted median/mean/mean (without convective events) of the full data set, the hatched line is the fit of the maximum IWC, and the dotted line is that of the minimum IWC, derived from 13 flights with gas phase H_2O measurements available (same as in Figure 3).

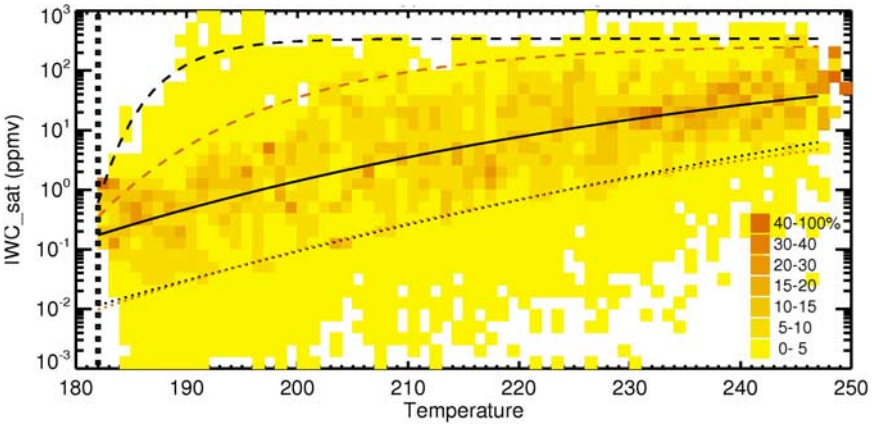

Figure 6. IWC frequencies of occurrence in 1-K temperature bins (52 flights, 97,103 data points). Solid line denotes the median. Dashed/dotted black curves denote the maximum/minimum IWC as in Figure 5, and dashed/dotted red curves denotes the maximum/minimum envelope of most frequent (>5%) IWC.

IWC, we therefore also provide the fitted mean excluding these five flights (green solid line in Figure 5) which is substantially different from that of all data. It has a similar slope to that of the median but is significantly higher. The median does not change significantly when the five flights are not considered. In Figure 5, the fit of the *Wang and Sassen* [2002] climatology is plotted again to illustrate the similarities and differences, the latter as an indicator of the accuracy of such approximations, for higher temperatures. However, it is apparent that a linear extrapolation to lower temperatures, as e.g., applied by *Kärcher and Voigt* [2006] due to the lack of data at that time, is inconsistent with our data set. A fit of the form $10^{(aT+c)}$ is not sufficient to describe the temperature dependence of IWC over the full range of temperatures in the upper tropopause globally.

[33] The mean IWC are used in the accompanying papers being relevant for the uptake of HNO_3 in cirrus clouds [*Krämer et al.*, 2008a] and contrail radiative forcing (Rodriguez et al., manuscript in preparation, 2008). They are further useful for parameterizations of cirrus clouds, e.g., in climate modeling. The median values are used in section 4 to discuss the probability of IWC occurrence in the context of temperature changes in the upper troposphere.

4. Discussion

[34] In section 3, we presented the ice water content derived from 10 campaigns in the Arctic, at midlatitudes, and in the tropics over the temperature range from 185 to 250 K. We used the mean and the median of the highly scattered data to describe the decrease of IWC by more than 2 orders of magnitude with decreasing temperature. The high scatter of IWC over several orders of magnitudes for a single temperature bin implies the question about the likelihood that a certain IWC occurs for a specific temperature. Figure 6 shows the frequency distribution of the IWC data set binned in 1 K temperature intervals. We define a core region where the frequency of occurrence exceeds 5%, which is confined by the red dashed (maximum) and dotted (minimum) lines; coefficients for these fit functions are given in Table 2. The minimum line coincides almost with that of the minimum detectable IWC as defined in section 3; thus the number of ambiguous data with very low IWC represents only a very low fraction of the full data set. We can then identify a core belt of about 2 orders of magnitude of mixing ratio around the median, with the characteristic strong decrease in IWC with temperature. Beyond this core, the frequency of IWC drops below 5% and can be attributed to data with low experimental confidence (IWC lower than the minimum limit) or specific phenomena (IWC higher than the maximum limit) as discussed in the following.

[35] Figure 7 shows the frequency distribution of IWC binned for the temperature range T > 205 K and T < 205 K, respectively. The distribution is calculated for the 28 flights when gas phase measurements are available; they are displayed for both methods using the gas phase measurement (IWC_{gas}) and the saturation RHi = 100% (IWC_{sat}) as a reference. Both methods, as Figure 7 demonstrates, yield the same peak values as well as the width and shapes are almost identical. This finding corroborates our previous assump-

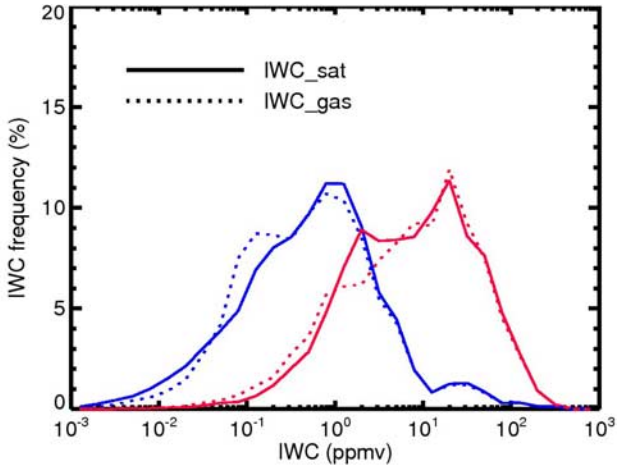

Figure 7. Frequency distribution of IWC binned for the temperature range T > 205 K (red) and T < 205K (blue). The distribution is calculated for the 28 flights when gas phase measurements are available; they are calculated for both methods using the gas phase measurement (dotted lines) and the RHi = 100% (solid line) as a reference.

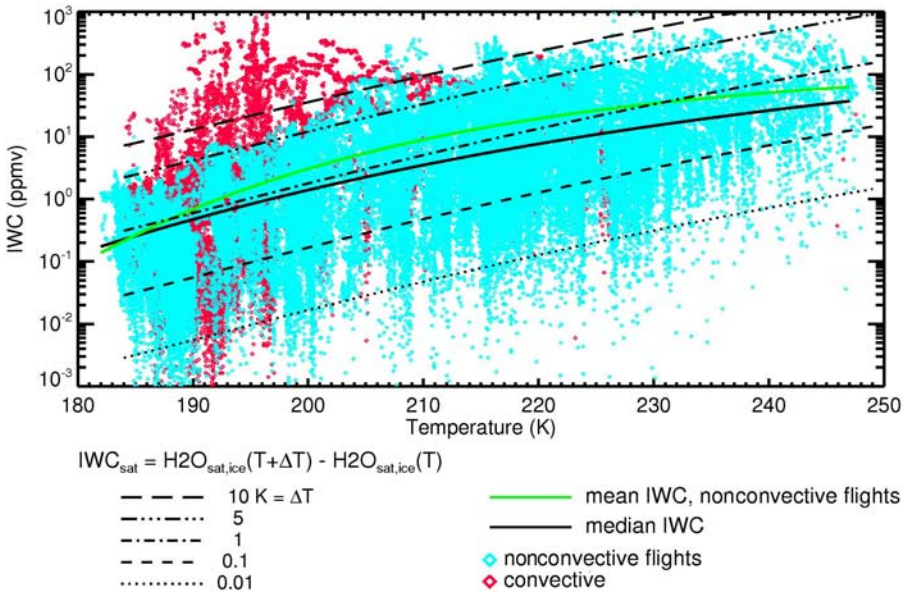

Figure 8. Ice water content (IWC) versus temperature as in Figure 5, but data observed during flights in the vicinity of deep convection are highlighted in red. Black lines represent IWC_{sat} according to *Marti and Mauersberger* [1993] for T+0.01, T+0.1K, T+1K, T+5K, and T+10K, respectively.

tion, that IWC calculated using the saturation mixing ratio yield, in this climatological study, almost the same mean values and distribution as using gas phase measurements instead. For a single measurement, however, both approaches may differ if supersaturation or subsaturation occurs.

[36] In Figure 8 we marked in red color those tropical flights which have been carried out in or in the vicinity of deep convection, i.e., the APE-THESEO flight on 9 March 1999, the TROCCINOX flight on 4 February 2005, and the SCOUT-O3 flights on 23, 29, and 30 November 2005. On these days, overshooting convection up to the cold point tropopause or even higher transported ice particles and water into this very cold region [*Stefanutti et al.*, 2004; *Chaboureau et al.*, 2007; *Vaughan et al.*, 2008]. The highest IWC have been observed in the upper parts of the anvil or in overshooting turrets of these convective systems. Details of the observations and the meteorological situation will be discussed in separate publications dedicated to these events [*Corti et al.*, 2008; *de Reus et al.*, 2008].

[37] From the discrimination of data in the two categories in Figure 8 (convective and nonconvective days) we can derive the following conclusions: First, besides regions of fresh deep convective events up the cold point region, also the upper envelope of the IWC of cirrus clouds is decreasing with decreasing temperature similar as the median and coincides almost with the upper limit of the core belt in Figure 6. Maximum IWC values at 190 K are 1–2 ppmv and thus about one order of magnitude lower than at 210 K temperature. Second, deep convection occasionally transports ice particles with an IWC much higher than this upper envelope into the tropopause region. The observed IWC of 10–100 ppmv (or higher) in these events may exceed the climatological IWC distribution of the core belt by more than one order of magnitude. This phenomenon is apparent also in the frequency distribution in Figure 7 as a second mode in the blue curves at high IWC, i.e., 10–100 ppmv. Thus, the SCOUT-O3 and TROCCINOX observations show that deep convection can transport substantial amounts of water into the upper TTL and even above the tropopause and thus moisten its environment [*Corti et al.*, 2008].

[38] In the following, we compare the temperature dependence of the IWC median with functions of the form $10^{(a/T+b)}$, the same type of formula as the approximated Clausius-Clapeyron equation which *Marti and Mauersberger* [1993] used to fit the ice saturation data from laboratory studies. Using this formula, we calculate curves of ice water contents $IWC_{sat} = H_2O_{sat,ice}(T+dT) - H_2O_{sat,ice}(T)$, with dT = 0.01, 0.1, 1, 5, and 10 K, which are overlaid on the IWC data set in Figure 8. For pressure, mean temperature-dependent values are used which are derived from averaged measured profiles. IWC_{sat} can be regarded as the maximum IWC of a cirrus cloud at a cooling of dT when the cooling process starts at RH_{ice} = 100%. This very simplified approach, however, only describes the net effect of the cloud life cycle, as a real cirrus particle forms in a cooling process and then may sediment and evaporate in subsaturated environment. The IWC of convective cirrus cannot be described by the simple approximation derived from $H_2O_{sat,ice}$; these clouds are formed by freezing of warmer liquid clouds nucleated at lower altitudes, while the in situ cirrus arise from deposition freezing which is correlated to $H_2O_{sat,ice}$. The mean of the IWC data (Figure 5) coincides best with IWC_{sat} at dT = 1 K for a large range of temperatures. In other words, on average the clouds are observed in air masses which have suffered a net cooling by approximately 1 K below the frost point temperature. On the one hand, the similarity of the temperature dependence of the measured mean IWC and the IWC_{sat} curves is not surprising since both phenomena are based on the same thermodynamical

processes, the first one observed in the atmosphere and the latter one based on laboratory experiments. On the other hand, from the large variability of IWC occurring in the real atmosphere for a specific temperature and the range of potential supersaturation one cannot a priori expect that the mean of our IWC data set is showing this similarity.

[39] The decrease of IWC with temperature is also visible in the minimum and maximum values of IWC. IWC_{sat} calculated for temperatures 5 K above the frost point represents an upper envelope for those IWC data not impacted by fresh convection, corresponding to the upper limit of the core belt in Figure 6. This implies that cirrus buildup induced from cooling of about 5 K is an approximate upper limit in the TTL, except in a convective case. The lower limit of the core belt are a composite of cirrus particles which either have suffered a very moderate cooling (0.1 K or less) or have sedimented from above and are in a decaying stage.

5. Conclusions

[40] A major result of this study is the climatology of cirrus ice water content derived from airborne in situ measurements in the Arctic, at midlatitudes and in the tropics. The temperature dependence of the IWC is determined for a large range down to 183 K and thus extends previous climatologies significantly to the low temperature range. The data set also includes low IWC below 0.1 ppmv which are not resolved in most previous climatologies but which are essential in particular for the very low temperatures. The mean and median of IWC as well as their maximum and minimum values show a steep decrease with temperature. This decrease can no longer be described by an extrapolation of previous midlatitude climatologies and requires fit functions which are nonlinear in the exponent. For the median, maximum, and minimum IWC we provide such fit functions whose coefficients are given in Table 2. These functions will be used in upcoming papers to discuss modeling of supersaturation in cirrus clouds and HNO_3 uptake on ice particles, and they are important input parameters in future process oriented studies as well as climate modeling.

[41] The fitted IWC curves are similar to functions of $IWC_{sat} = H_2O_{sat,ice}(T+dT) - H_2O_{sat,ice}(T)$ calculated by means the empirical formula for the water saturation pressure by *Marti and Mauersberger* [1993]. The similarity between the averaged atmospheric data and such fundamental principles shows that despite the large variability our data set obtained in different regions of the Earth is representative on a global scale.

[42] Comparing the data with IWC_{sat}, the median IWC in cirrus clouds can be attributed to a net cooling of 1 K. Cirrus particles growing under moderate cooling rates are likely to sediment, thus resulting in a drying of the UTLS. In particular clouds with a low IWC, distributed to only few particles as occurring in very cold air masses, have a high dehydration potential [*Luo et al.*, 2003].

[43] However, data from a small subset of tropical flights, which were obtained in the vicinity of deep convection, show significantly higher IWC than the climatological IWC distribution at low temperatures. These observations imply that ice and water can bypass the cold trap in the upper troposphere via convection and moisten the air at higher altitudes.

[44] **Acknowledgments.** We would like to thank R. Bauer, J. Beuermann, M. Bläsner, O. Bujok, N. Eicke, A. Mangold, S. Rohs, S. Schlicht, G. Shur, F. H. Silva dos Santos, A. Schönfeld, V. Tan, and M. Zöger who were involved in the experimental work during the different campaigns, as well as the aircraft teams of DLR Oberpfaffenhofen, GfD Hohn, enviscope Frankfurt, and MDB Moscow and the coordinators of the different field experiments. Funding for the campaigns was granted by the BMBF within the Ozonforschungsprogramm and the program "Angewandte Klima- und Atmosphärenforschung," by the EU DG XII within Framework Programmes 5 and 6, and by ESA within the ENVISAT validation program. Water vapor measurement by FLASH and data preparation was supported by the Russian Foundation for Basic Research grants 06-05-64165-a and 07-05-00486-a.

References

Borrmann, S., S. Solomon, J. E. Dye, and B. Luo (1996), The potential of cirrus clouds for heterogeneous chlorine activation, *Geophys. Res. Lett.*, *23*, 2133–2136, doi:10.1029/96GL01957.

Chaboureau, J.-P., J.-P. Cammas, J. Duron, P. J. Mascart, N. M. Sitnikov, and H.-J. Voessing (2007), A numerical study of tropical cross-tropopause transport by convective overshoots, *Atmos. Chem. Phys.*, *7*, 1731–1740.

Corti, T., et al. (2008), Unprecedented evidence for overshooting convection hydrating the tropical stratosphere, *Geophys. Res. Lett.*, *35*, L10810, doi:10.1029/2008GL033641.

de Reus, M., et al. (2008), Evidence for ice particles in the tropical stratosphere from in-situ measurements, *Atmos. Chem. Phys. Discuss*, *8*, 19,313–19,355.

Forster, P., et al. (2007), Changes in atmospheric constituents and in radiative forcing, in *Climate Change*, edited by S. Solomon et al., pp. 129–220, Cambridge Univ. Press, Cambridge, U. K.

Fu, Q. (1996), An accurate parameterization of the solar radiative properties of cirrus clouds for climate models, *J. Clim.*, *9*, 2058–2082, doi:10.1175/1520-0442(1996)009<2058:AAPOTS>2.0.CO;2.

Fueglistaler, S., and M. B. Baker (2006), A modelling study of the impact of cirrus clouds on the moisture budget of the upper tropopause, *Atmos. Chem. Phys.*, *6*, 1425–1434.

Gayet, J.-F., V. Shcherbakov, H. Mannstein, A. Minikin, U. Schumann, J. Ström, A. Petzold, J. Ovarlez, and F. Immler (2006), Microphysical and optical properties of mid-latitude cirrus clouds observed in the southern hemisphere during INCA, *Q.J.R. Meteorol. Soc.*, *132*, 2721–2750.

Heymsfield, A. J. (1986), Ice particles observed in a cirriform cloud at −83°C and implications for polar stratospheric clouds, *J. Atmos. Sci.*, *43*, 851–855, doi:10.1175/1520-0469(1986)043<0851:IPOIAC>2.0.CO;2.

Heymsfield, A. J., and G. M. McFarquhar (2002), Mid-latitude and tropical cirrus: Microphysical properties, in *Cirrus*, edited by D. K. Lynch et al., pp. 78–101, Oxford Univ. Press, New York.

Heymsfield, A. J., and C. M. R. Platt (1984), A parameterization of the particle spectrum of ice clouds in terms of the ambient temperature and the ice water content, *J. Atmos. Sci.*, *41*, 846–855, doi:10.1175/1520-0469(1984)041<0846:APOTPS>2.0.CO;2.

Jensen, E. J., et al. (2005), Formation of a tropopause cirrus layer observed over Florida during CRYSTAL-FACE, *J. Geophys. Res.*, *110*, D03208, doi:10.1029/2004JD004671.

Kärcher, B., and C. Voigt (2006), Formation of nitric acid/water ice particles in cirrus clouds, *Geophys. Res. Lett.*, *33*, L08806, doi:10.1029/2006GL025927.

Kley, D., et al. (2000), SPARC assessment of water vapour in the stratosphere and upper troposphere, *SPARC Rep. 2*, World Meteorol. Org., Geneva.

Krämer, M., and A. Afchine (2004), Sampling characteristics of inlets operated at low U/U0 ratios: New insights from computational fluid dynamics (CFX) modeling, *J. Aerosol Sci.*, *35*(6), 683–694, doi:10.1016/j.jaerosci.2003.11.011.

Krämer, M., C. Schiller, C. Voigt, H. Schlager, and P. Popp (2008a), A climatological view to HNO3 partitioning in cirrus clouds, *Q. J. R. Meteorol. Soc.*, *134*, 905–912, doi:10.1002/qj.253.

Krämer, M., et al. (2008b), Ice supersaturations and cirrus cloud crystal numbers, *Atmos. Chem. Phys. Discuss*, in press.

Luo, B. P., et al. (2003), Dehydration potential of ultrathin clouds at the tropical tropopause, *Geophys. Res. Lett.*, *30*(11), 1557, doi:10.1029/2002GL016737.

MacKenzie, A. R., et al. (2006), The tropopause and hygropause in the equatorial Indian Ocean during February and March 1999, *J. Geophys. Res.*, *111*, D18112, doi:10.1029/2005JD006639.

Marti, J., and K. Mauersberger (1993), A survey and new measurements of ice vapor pressure at temperatures between 170 and 250 K, *Geophys. Res. Lett.*, *20*, 363–366, doi:10.1029/93GL00105.

May, R. D. (1998), Open-path, near-infrared tunable diode laser spectrometer for atmospheric measurements of H_2O, *J. Geophys. Res.*, *103*, 19,161–19,172, doi:10.1029/98JD01678.

McFarquhar, G. M., and A. J. Heymsfield (1997), Parameterization of tropical cirrus ice crystal size distributions and implications for radiative transfer: Results from CEPEX, *J. Atmos. Sci.*, *54*, 2187–2200, doi:10.1175/1520-0469(1997)054<2187:POTCIC>2.0.CO;2.

Ovarlez, J., et al. (2002), Water vapour measurements inside cirrus clouds in Northern and Southern hemispheres during INCA, *Geophys. Res. Lett.*, *29*(16), 1813, doi:10.1029/2001GL014440.

Schiller, C., A. Afchine, N. Eicke, H. Fischer, A. Giez, P. Konopka, H. Schlager, F. Wienhold, and M. Zöger (1999), Total water measurements in the tropopause region during the Polar Stratosphere Aerosol Experiment I, 1997, *Geophys. Res. Lett.*, *26*, 2219–2222, doi:10.1029/1999GL900337.

Schlicht, S. (2006), Untersuchung zur Wasser-Partitionierung in Zirruswolken (in German), Ph.D. thesis, Univ. of Wuppertal, Wuppertal, Germany.

Sitnikov, N. M., V. A. Yushkov, A. A. Afchine, L. I. Korshunov, V. I. Astakhov, A. E. Ulanovskii, M. Kraemer, A. Mangold, C. Schiller, and F. Ravegnani (2007), The FLASH instrument for water vapor measurements on board the high-altitude airplane, *Instrum. Exp. Tech.*, *50*(1), 113–121, doi:10.1134/S0020441207010174.

Stefanutti, L., et al. (2004), The APE-THESEO tropical campaign, *J. Atmos. Chem.*, *48*, 1–33, doi:10.1023/B:JOCH.0000034509.11746.b8.

Vaughan, G., C. Schiller, A. R. MacKenzie, K. Bower, T. Peter, H. Schlager, N. R. P. Harris, and P. T. May (2008), SCOUT-O3/ACTIVE: High-altitude aircraft measurements around deep tropical convection, *Bull. Am. Meteorol. Soc.*, *89*, 647–662, doi:10.1175/BAMS-89-5-647.

Wang, Z., and K. Sassen (2002), Cirrus cloud microphysical property retrieval using lidar and radar measurements. Part II: Midlatitude cirrus microphysical and radiative properties, *J. Atmos. Sci.*, *59*, 2291–2303, doi:10.1175/1520-0469(2002)059<2291:CCMPRU>2.0.CO;2.

Zöger, M., et al. (1999), Fast in situ stratospheric hygrometers: A new family of balloonborne and airborne Lyman-α photofragment fluorescence hygrometers, *J. Geophys. Res.*, *104*, 1807–1816, doi:10.1029/1998JD100025.

A. Afchine, M. Krämer, C. Schiller, and N. Spelten, Institut für Chemie und Dynamik der Geosphäre 1, Forschungszentrum Jülich, D-52425 Stratosphäre, Germany. (c.schiller@fz-juelich.de)

N. Sitnikov, Central Aerological Observatory, 141700 Dolgoprudny, Russia.